PERGAMON

Journal of Structural Geology 21 (1999) 161–177

JOURNAL OF STRUCTURAL GEOLOGY

Finite-element modelling of single-layer folding in elasto-viscous materials: the effect of initial perturbation geometry

N.S. Mancktelow *

Geologisches Institut, ETH-Zentrum, CH-8092 Zürich, Switzerland

Received 17 March 1998; accepted 7 October 1998

Abstract

The influence of periodic, isolated bell-shaped and random initial perturbations on single-layer fold amplification was numerically modelled for a wide range of elasto-viscous material properties. The results from this finite-element modelling (FEM) are markedly different from previous finite-difference (FLAC) models, but similar to analogue scale-models. For periodic perturbations, only the introduced waveform is amplified into folds, even for an initial wavelength much shorter or longer than the fastest growing 'dominant' wavelength. Hinge and inflection points remain fixed to the same material points and there is no hinge migration to allow development of the dominant wavelength. Enhanced elastic behaviour increases the growth rate of shorter wavelength components and hence modifies the final fold shape, but hinge or inflection points still remain fixed. For initial isolated bell-shaped perturbations, a slow serial sideways propagation of folding along the layer leads to the eventual development of an internally periodic fold packet of near constant amplitude at high values of shortening ($>50\%$). Increased elastic or non-linear power law viscous behaviour promotes localization about the initial isolated perturbation. Even for random initial irregularities, the final high-amplitude fold shape is only quasi-periodic and still shows the influence of the initial perturbation geometry. The maximum amplitude of these initial irregularities also influences the final fold shape, especially when the growth rate of the folds is low. For the same viscosity contrast, smaller initial amplitude promotes growth of long wavelength components producing final shapes similar to those developed in higher viscosity ratio experiments. Increased elastic behaviour promotes shorter wavelengths, faster growth rates and greater wavelength selectivity, resulting in more regular periodic forms that are less influenced by initial perturbation amplitude. However, in all cases investigated, the initial perturbation geometry still exerts an influence on the finite fold shape and the irregular, only quasi-periodic form of many natural folds reflects this initial irregularity control.

1. Introduction

Although rocks, in common with all materials, show both short-term elasticity and longer-term viscous creep, theoretical and numerical studies of folding have generally considered only limited combinations of the full behaviour. Biot (1959, 1965) developed the basic principles for a comprehensive approach but application has been hindered by the inherent complexity and worked examples have only been presented for various combinations of elastic or incompressible viscous materials (e.g. Biot, 1959, 1961; Biot et al., 1961; Biot and Odé, 1962). The coefficients of the governing set of equations for folding of elasto-viscous materials are not necessarily symmetric and this important difficulty only disappears for isotropic incompressible materials (Biot and Odé, 1962). Results calculated from Biot's equations for the reduced incompressible viscous case show (relatively minor) divergence from exact infinitesimal results derived specifically for incompressible viscous materials (e.g. Fletcher, 1974, 1977; Smith, 1975), which also raises questions about the exactitude of the general theory.

Partly due to this lack of a usable theoretical basis, the assumption has generally been made in the past that, for slow natural deformation rates on the order of 10^{-14} s^{-1}, viscous behaviour dominates and that the elastic component exerts little influence on the observed fold geometry (e.g. Biot, 1961). The correspondence between purely viscous theoretical and numerical models and slowly deformed analogue scale-models, in which the materials are truly elasto-viscous,

* Correspondence: Tel.: +41-1-632-3671; fax: +41-1-632-1030; e-mail: neil@erdw.ethz.ch

0191-8141/99/$ - see front matter
PII: S0191-8141(98)00102-3

would support this assumption. However, the proposal has certainly not been fully tested, and the possible importance of elastic behaviour in the initial stages of folding for introducing both shorter wavelength components and greater spatial variability has been emphasized by several authors (e.g. Price and Cosgrove, 1990; Hunt et al., 1996a).

A recent paper by Zhang et al. (1996) that considered single-layer folding of elasto-viscous (and elasto-plastic) materials using a finite-difference FLAC code (Fast Lagrangian Analysis of Continua, Cundall and Board, 1988) reported results that are markedly different from both existing viscous theory and analogue scale-models. In their numerical models, a wavelength close to the 'dominant' (i.e. fastest growing) wavelength, as determined by viscosity contrast and layer thickness, was established at higher strain ($>10\%$ shortening) even when the initial periodic perturbation wavelength was much shorter. For an isolated initial perturbation, they found that folding propagated rapidly along the layer to again establish a nearly periodic form approaching the dominant wavelength. These results suggest that the shape of initial irregularities has only a subordinate influence on finite amplitude fold geometry. Their models also require that hinge migration occurs during fold amplification, to establish a near dominant wavelength different from the initial perturbation wavelength. This result would invalidate the primary assumption of most published numerical studies that have considered perfectly periodic initial irregularities (e.g. Dieterich and Carter, 1969; Stephansson and Berner, 1971; and many others), namely that only a single half-wavelength segment with planar boundary conditions need be modelled. This can only hold true if fold hinges and inflection points remain fixed to the same material points. Since wavelength components develop that were not present in the initial perturbation, the results of Zhang et al. (1996) can also not be reproduced by an analysis involving linear superposition of Fourier components amplifying independently (e.g. Biot, 1961; Mancktelow and Abbassi, 1992).

The present paper studies the growth of single-layer folds from an initial small amplitude perturbation using finite-element modelling (FEM). Model parameters are the same as used by Zhang et al. (1996) and material properties are chosen to cover the range of expected rock behaviour, including non-linear power-law viscosity with stress exponents up to 5. The aim was to replicate either the FLAC results or the analogue scale-model results of Abbassi and Mancktelow (1992). The FEM results are effectively identical to those from the analogue scale-modelling and do not corroborate the earlier FLAC models. Although study of simplified periodic or isolated initial perturbation forms provides an excellent basis for understanding the mechanisms of finite amplitude folding, initial perturbations in most natural rock layers are unlikely to be so regular. Indeed, it is commonly assumed that periodic folds of dominant wavelength develop from a random distribution of original irregularities in the layer surface. This possibility has been investigated in a series of experiments with perturbations of differing maximum initial amplitudes, for a range of effective viscosity contrasts and both linear and power-law (elasto-) viscous rheologies. Even for such random initial irregularities, the finite amplitude shapes are still clearly influenced by the initial input form and the observed lack of strict periodicity in natural folds (e.g. Sherwin and Chapple, 1968; Cobbold, 1976; Fletcher and Sherwin, 1978; Price and Cosgrove, 1990) probably reflects initial perturbation influence more than localization due to rheological effects (e.g. Hunt et al., 1996a,b; Whiting and Hunt, 1997).

2. Previous work

The body of published theoretical and experimental work on single-layer folds is very large, but the recent numerical work of Zhang et al. (1996) appears to be the first attempt to consider finite amplitude single-layer folding, where both layer and matrix are compressible elasto-viscous materials. Previous analytical and numerical studies have all considered some combination of simpler rheologies: e.g. elastic layer in an elastic matrix (e.g. Gough et al., 1940; Goodier, 1946), viscous layer in a viscous matrix—both linear and non-linear—(e.g. Biot, 1959; Biot and Odé, 1962; Ramberg, 1963; Dieterich and Carter, 1969; Parrish, 1973; Hudleston and Stephansson, 1973; Fletcher, 1974, 1977; Smith, 1975; Cobbold, 1977; Hudleston and Lan, 1993; and many others), elastic layer in a viscous matrix (e.g. Biot, 1961, 1965), and most recently elastic layer in an elasto-viscous matrix (e.g. Wilson and Vinson, 1983; Hunt et al., 1996a,b; Bhalerao and Moon, 1996a,b; Whiting and Hunt, 1997). Excellent summaries of the analytical approach to single-layer folding are given in Biot (1961, 1965) and Johnson and Fletcher (1994). First-order analytical results for incompressible viscous materials provide a theoretical basis for understanding fold selectivity and initial growth, and their extension to second- (Fletcher, 1979) and third-order (Johnson and Fletcher, 1994) also allows an accurate description of fold growth to small but finite limb dips ($<\sim 20^\circ$). This, of course, is provided that a more realistic elasto-viscous description does not lead to any fundamental difference in behaviour. Analogue scale-modelling would suggest otherwise, since the initial growth rates and overall geometry of single layer folding appears to be broadly consistent

with the predictions of first-order theory (e.g. Mancktelow and Abbassi, 1992).

3. Method

The FEM modelling is based on the commercial package MARC–Mentat. Mentat represents the front-end graphic user interface, allowing interactive mesh generation, boundary condition and material property definition, etc., as well as post-processing and graphical representation of the results. In theory, the whole process of model generation, job submission and result analysis should be possible in interactive mode, but in practice it is more effective to first generate a standard input file for a given planar layer thickness, standard material properties and boundary conditions with Mentat, modify this standard file for each submission to the main FEM program MARC, and then analyse the generated post-processing file again with Mentat.

Time-stepping for viscous creep is automatically modified within the program to maintain given tolerances. In all the models presented here, these tolerances were that the creep strain in any one increment never exceeds 0.5 of the elastic strain (a necessary constraint to maintain numerical stability), and that the stress change during the increment does not exceed 0.1 of the current stress. Since the elastic strain in the models is generally small (for stresses on the order 10^0–10^2 MPa at imposed strain rates of 10^{-14} s^{-1}), the time steps are also small and become smaller for lower viscosities. Most models involved on the order of 3000–30,000 increments for between 20 and 70% total shortening, depending on material properties (especially whether linear or power-law viscous rheology). This is an important difference from previously published, purely viscous FEM models of folding where step sizes were commonly on the order of 1–5% shortening (e.g. Stephansson and Berner, 1971; Cobbold, 1977; Casey and Huggenberger, 1985). The tolerance on convergence in each step was left at the default value, namely that the sum of the residual forces may not exceed 0.1 of the reaction forces, and this value was only ever approached at the end of large strain runs (e.g. $>60\%$ shortening), when the mesh was locally very distorted. Further details on methods and element geometry, as well as postal and internet contact addresses of the distributor, are given in the Appendix.

Table 1
Values relevant to Figs. 3 and 9, after Zhang et al. (1996). Newtonian linear viscosity, strain-rate not stated

R	E_l [Pa]	E_m [Pa]	η_l [Pa s]	η_m [Pa s]
20	3.5×10^{10}	1.75×10^{9}	1×10^{20}	5×10^{18}
50	3.5×10^{10}	7.00×10^{8}	1×10^{20}	2×10^{18}
100	3.5×10^{10}	3.50×10^{8}	1×10^{20}	1×10^{18}
200	3.5×10^{10}	1.75×10^{8}	1×10^{20}	5×10^{17}

4. Material properties

Rock rheology is modelled as a Maxwell elasto-viscous material, represented by the in-series addition of a compressible linear elastic element and an incompressible linear or power-law viscous element. For the elastic component, the Poisson's ratio is taken as 0.25 for both layer and matrix, which was also the value used in the models of Zhang et al. (1996). Values for other parameters used for the different runs of the current study (for definitions, see the Appendix are listed in Tables 1–5 and are within the range established for natural rocks (e.g. see appendix of Turcotte and Schubert, 1982). For direct comparison, runs were also made with the same parameters employed by Zhang et al. (1996), which are listed in Table 1, with an imposed strain rate of 10^{-14} s^{-1}. These authors maintained the same ratio between layer and matrix for both elastic and viscous parameters (i.e. in the range from 20:1 to 200:1). However, the measured range in Young's modulus for natural rocks is only about a single order of magnitude. To compare with natural and analogue scale-model folding, the ratio in Young's moduli was therefore taken as 1:1 (Table 3), 2:1 (Tables 2, 3 and 4) or 10:1 (Table 5) between layer and matrix, with values in the range 1×10^9–6×10^{10} Pa. Viscosities employed (10^{18}–10^{22} Pa s) were generally higher than in the earlier study but details of

Table 2
Values relevant to Figs. 1, 2, 10, 11a, 16 and 17. Newtonian linear viscosity

R	E_l [Pa]	E_m [Pa]	η_l [Pa s]	η_m [Pa s]	$d\varepsilon/dt$ [s^{-1}]	De_l	De_m
20	6×10^{10}	3×10^{10}	3.33×10^{21}	1.67×10^{20}	1×10^{-14}	1.4×10^{-3}	1.4×10^{-4}
50	6×10^{10}	3×10^{10}	8.33×10^{21}	1.67×10^{20}	1×10^{-14}	3.5×10^{-3}	1.4×10^{-4}
100	6×10^{10}	3×10^{10}	8.33×10^{21}	8.33×10^{19}	1×10^{-14}	3.5×10^{-3}	6.9×10^{-5}
200	6×10^{10}	3×10^{10}	1.67×10^{22}	8.33×10^{19}	1×10^{-14}	7.0×10^{-3}	6.9×10^{-5}

Table 3
Values relevant to Figs. 6, 7, 13, 19 and 20. Newtonian linear viscosity

$\varepsilon_e/\varepsilon_c$	E_l [Pa]	E_m [Pa]	η_l [Pa s]	η_m [Pa s]	$d\varepsilon/dt$ [s^{-1}]	De_l	De_m
2.86	1×10^{9}	1×10^{9}	1×10^{22}	1×10^{20}	1×10^{-14}	2.5×10^{-1}	2.5×10^{-3}
0.43	5×10^{9}	5×10^{9}	1×10^{22}	1×10^{20}	1×10^{-14}	5.0×10^{-2}	5.0×10^{-4}
0.18	1×10^{10}	5×10^{9}	1×10^{22}	1×10^{20}	1×10^{-14}	2.5×10^{-2}	5.0×10^{-4}
0.03	5×10^{10}	5×10^{9}	1×10^{22}	1×10^{20}	1×10^{-14}	5.0×10^{-3}	5.0×10^{-4}

$\varepsilon_e/\varepsilon_c$ is the ratio between equivalent elastic and creep strain in the inner arc of the models of Fig. 6, at log. strain $=-0.2$.

Table 4
Values relevant to Figs. 11b and 18. Non-Newtonian power-law viscosity

R	E_l [Pa]	E_m [Pa]	A_l	n_l	A_m	n_m	$d\varepsilon/dt$ [s^{-1}]
50	6×10^{10}	3×10^{10}	6.400×10^{-40}	3	8×10^{-35}	3	1×10^{-14}
50	6×10^{10}	3×10^{10}	1.024×10^{-56}	5	8×10^{-35}	3	1×10^{-14}

NB. the constants are scaled to more reasonable units (MPa etc.) for program input.

strain rate(s) were not listed in Zhang et al. (1996), so that direct comparison of flow stress levels is not possible. This is important, since it is the non-dimensional Deborah number, De, equal to the ratio of the stress magnitude to the elastic shear modulus (i.e. viscosity × strain rate/shear modulus) that is important in scaling elasto-viscous Maxwell-type rheologies (e.g. Poliakov et al., 1993). This ratio also determines the maximum stable size of steps for the numerical models, so that if there is no significant difference in behaviour it is more efficient to employ higher viscosities (or higher strain rates) and/or lower elastic moduli. Values of De for layer (De_l) and matrix (De_m) are listed Tables 1–5. Poliakov et al. (1993) estimate limits for the Deborah number in the upper crust to be 10^{-4}–10^{-3} and 10^{-3}–10^{-2} for the upper mantle (i.e. the levels where the elastic effects are expected to be greatest) and note that flow exhibits viscous behaviour for $De < 10^{-2}$. This is qualitatively confirmed in Table 3. On the innermost arc of the periodic folds developed in these models (see Fig. 6 later), the elastic strain is very small relative to the viscous creep strain for $De < 10^{-2}$. The range of values of De employed in the current series of numerical experiments is 7×10^{-5} to 0.25. Rheologies with still lower values of De are effectively viscous and have been considered in many previous numerical modelling studies (e.g. Dieterich and Carter, 1969; Hudleston and Stephansson, 1973; Parrish, 1973; Parrish et al., 1976; Cobbold, 1977).

The effect of non-linear viscous behaviour according to the power-law relationship $\dot{\varepsilon} = A\sigma^n$, with stress exponents of 3 for the matrix and 3 and 5 for the layer was also investigated (Table 4). In particular for higher n values, it is necessary to use units of a more realistic scale (e.g. MPa, 10^{10} s, etc.) than standard SI units for program input to avoid numeric under- and overflow, particularly in the pre-exponential constant A. The FEM program MARC assumes that the material properties entered were determined in uniaxial tests and generalizes the result to any geometry in terms of the second invariants of stress and strain (or effective shear stress and effective strain rate, see Ranalli, 1995, p.76). For plane strain geometry and incompressible linear viscous rheology, where $\sigma_{xx} = 4\eta\dot{\varepsilon}_{xx}$ and the deviatoric stress $\sigma'_{xx} = 2\eta\dot{\varepsilon}_{xx}$, the viscosity $\eta = 1/(3A)$, where A is the pre-exponential constant in the general power-law relationship above. Deviatoric stresses are in the range of ~2–5 MPa in the matrix and 100–400 MPa in the layer. These values are thought to be fairly realistic; common values quoted for the range of averaged stress in the lithosphere are 10–150 MPa (e.g. Hanks and Raleigh, 1980).

5. Model geometry and boundary conditions

The overall model dimensions were exactly as employed by Zhang et al. (1996). The length was 198 units, the width 128 units, and the layer 2 units thick. The contact between layer and matrix was 'welded' (i.e. non-slipping). Between 3300 and 10,400 quadratic

Table 5
Values relevant to Fig. 12. Newtonian linear viscosity

R	E_l [Pa]	E_m [Pa]	η_l [Pa s]	η_m [Pa s]	$d\varepsilon/dt$ [s^{-1}]	De_l	De_m
50	5×10^{10}	5×10^{9}	5×10^{19}	1×10^{18}	1×10^{-12}	2.5×10^{-3}	5.0×10^{-4}
100	5×10^{10}	5×10^{9}	1×10^{22}	1×10^{20}	1×10^{-14}	5.0×10^{-3}	5.0×10^{-4}

elements were employed and the mesh progressively refined to either side of the layer, six elements representing the layer width. Models were deformed in plane strain with a constant natural strain rate of 1×10^{-14} s^{-1} imposed at the boundaries (or in one case 10^{-12} s^{-1}, see Table 5). The necessary (time-dependent) velocity boundary condition was applied to the left and right planar sides of the rectangular mesh and, in general, the upper and lower boundaries were left unconstrained. However, models with an initial sinusoidal perturbation and viscosity ratios of 100:1 and 200:1 were also rerun with the y coordinates of the upper and lower surfaces constrained to maintain perfect pure shear. It is these results that are presented in Fig. 1(a). The additional constraint (slightly) dampens the boundary effects on the folding layer, but because the materials are compressible, it also produces weak edge effects in the matrix at the four corners. For most models, the y coordinate of the mid-point of each side was held fixed but in models with a centre of symmetry (i.e. those of Figs. 1(b) and 2, with an inflection point to the initial periodic perturbation at the central point), this central point was fixed.

6. Perturbation geometry

Three different perturbation geometries were investigated: periodic, isolated bell-shaped and random. The first two cases were chosen for direct comparison with both the previous FLAC study and the analogue scale-modelling of Abbassi and Mancktelow (1992), whereas the random initial variation in layer thickness may be more directly comparable with the development of many natural folds. As noted earlier, the layer thickness was in all cases 2 units and the length 198 units. The periodic perturbation was in most models of the

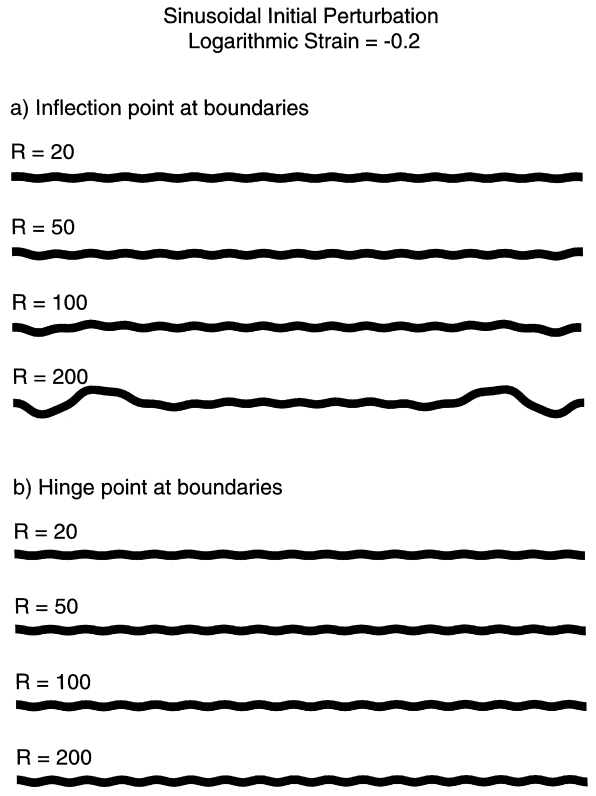

Fig. 1. FEM models of single layer buckling in elasto-viscous materials with the same initial geometries and viscosity contrasts as Fig. 3 (material properties listed in Table 2). In (a) an inflection point of the initial periodic perturbation is at the boundaries, the same as in Fig. 3, whereas in (b) it is a hinge point, which gives better boundary conditions because the axial plane remains vertical and planar throughout the experiments. The R-values give viscosity ratios and all examples are for $\varepsilon = -0.2$ bulk logarithmic shortening (~18% shortening). No significant difference in results is obtained if the parameters of Table 1 from Zhang et al. (1996) are used, with a strain rate of 10^{-14} s^{-1}.

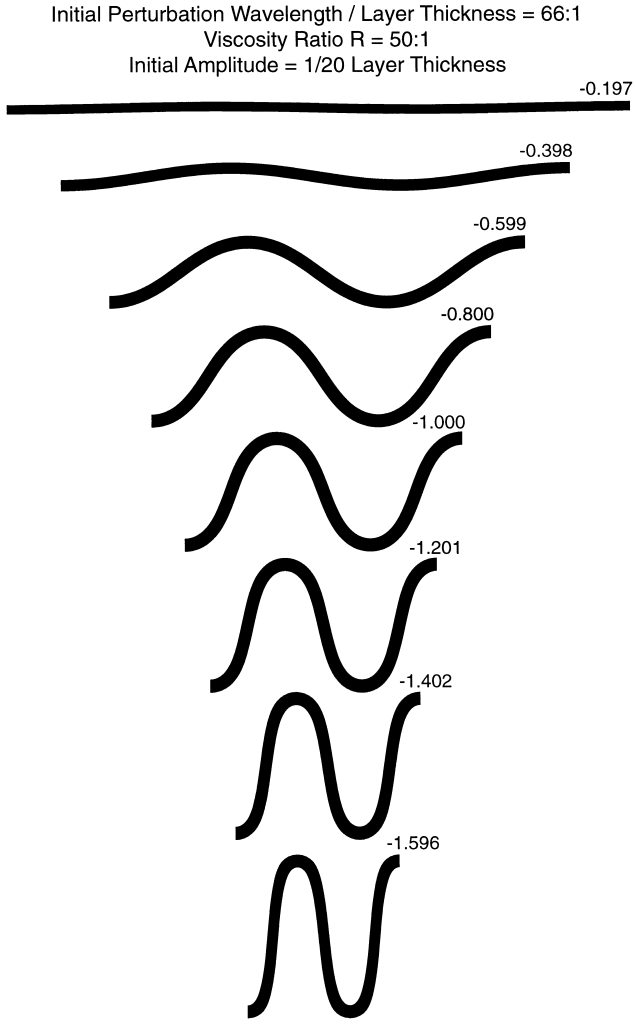

Fig. 2. Amplification of an initial periodic perturbation with wavelength 66 times layer thickness. Other parameters are identical to those with $R = 50$ in Fig. 1(b) (Table 2).

form $0.1\cos(\pi x/6)$, that is a total of 33 half-wavelengths of amplitude 0.1 in the length of the model, corresponding to an initial wavelength to thickness ratio of 6:1. This is lower than the theoretical dominant wavelengths for incompressible linear viscous materials, which are 10.3, 13.4, 16.5 and 20.6 times layer thickness for the viscosity ratios of 20, 50, 100, and 200 employed in the models (Fletcher 1974, 1977; see Fig. 5a). Models were initially calculated with perturbation inflection points at the boundaries and a hinge in the centre (cosinus form) for direct comparison with Zhang et al. (1996). However, since inflection points do not lie on a plane of constant x-displacement, marked edge effects occur at higher viscosity contrasts (Fig. 1a). These effects can be avoided in models with hinges at the boundaries and an inflection point at the centre (sinus form, Fig. 1b), as employed in most previous studies (e.g. Dieterich and Carter, 1969; Stephansson and Berner, 1971; Parrish, 1973; Stephansson, 1974; Hudleston and Lan, 1993). One model was also run with an initial wavelength to thickness ratio of 66:1, much larger than the dominant wavelength (Fig. 2).

The exact geometry of the initial isolated perturbations is not given in Zhang et al. (1996). Their perturbations A, B, and C are stated to be similar to the corresponding mathematically-defined Perturbation A, B and C of Abbassi and Mancktelow (1992), although it is clear from inspection of their figures that at least their perturbation C is not a perfect bell-shape. These slight differences are not insignificant. They will be reflected in the Fourier wavelength components originally present in the perturbation and since the amplification during buckle folding is wavelength specific, minor differences can become important at higher fold amplitudes. In this study, the initial perturbation shapes correspond exactly to those of Perturbation A, B and C in Abbassi and Mancktelow (1992), that is a bell-shape of the form $y = b/[1 + (x/a)^2]$ with values of a chosen to give average wavelengths of 8, 16 and 32 times layer thickness (Perturbation A, B, and C, respectively). Perturbations in the present study had an initial amplitude of $b = 0.1$ (1/20 of layer thickness) or $b = 1$ (1/2 of layer thickness), the latter being the same as in the earlier analogue scale-model studies.

In nature, initial perturbations in the rock layering will only rarely be approximately periodic (e.g. ripple marks), and are usually much more irregular, approaching an uncorrelated random distribution. A series of model experiments was therefore also performed with random distributions of initial irregularities of different maximum amplitudes. Segments of random distributions were repeated in some models, to establish if there is always a local control on fold shape by initial perturbation shape, even for random distributions.

7. Results

The deformed shapes of single layers with an initial sinusoidal perturbation and (linear) viscosity ratios of 20, 50, 100 and 200:1 are reproduced in Fig. 3 from Zhang et al. (1996) for comparison with the results of the current study in Fig. 1. In Fig. 1(a) the initial perturbation had inflection points at the boundary, corresponding to the initial conditions of Fig. 3, whereas in Fig. 1(b) the same initial perturbation geometry is shifted in phase by a quarter wavelength so that hinge points occur at the boundary, minimizing edge effects. The results in Figs. 1 and 3 are clearly very different. The original 33 half-wavelengths in the introduced perturbation are retained throughout the folding history in the FEM models of Fig. 1. In contrast to Fig. 3, there is no tendency for hinge migration and the consequent development of wavelengths closer to the dominant wavelength appropriate to the material properties. Hinge and inflection points remained fixed to the same material points (Fig. 4a). This implies that the wavenumber of any additional sinusoidal components that may develop with increasing amplification, to produce a fold shape different from the introduced perfectly similar fold geometry, must be an integer multiple of the initial wavenumber (as demonstrated analytically by Johnson and Fletcher, 1994). If plotted in a Lagrangian co-ordinate system relative to the initial x-coordinates of the nodes, the shape of the central surface remains close to perfectly sinusoidal (Fig. 4b), at least for the low limb dips attained in the models of Fig. 1(b) ($< 3^\circ$). The variation in nodal x-coordinate position away from the position corresponding to a homogeneous strain also describes a

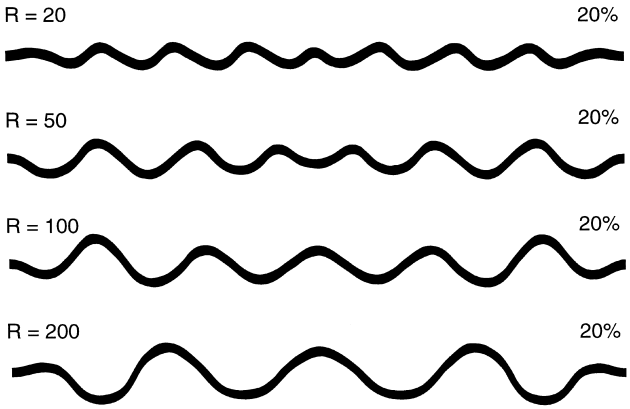

Fig. 3. Reproduction of Fig. 2a from Zhang et al. (1996) showing the geometry of their FLAC models for buckled single layers in elasto-viscous materials, developed from initial periodic perturbations with initial amplitude 1/20 of layer thickness and initial wavelength 6 times layer thickness. The R-values give viscosity ratios and all examples are for 20% bulk shortening. Material parameters are listed in Table 1.

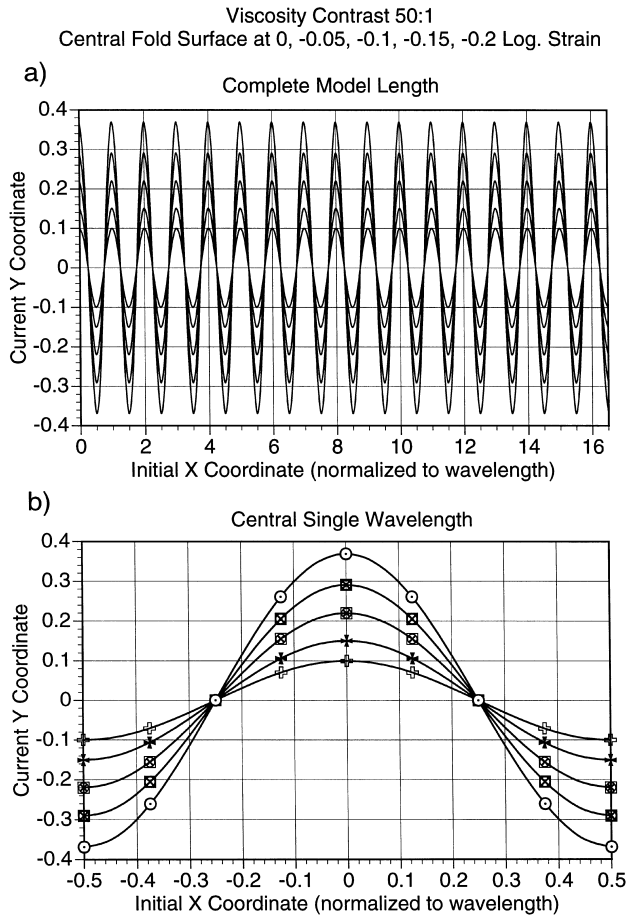

Fig. 4. (a) Shape of the central surface (i.e. material points initially defining the mid-line of the layer) that develops from a periodic initial perturbation for $R = 50$ and boundary conditions of Fig. 1(b). The shape is plotted relative to the initial x-position of material (nodal) points, from which it can be seen that the inflection and hinge points of the fold always remain fixed to the same material points. (b) One wavelength of the same fold train, with sinusoidal curves plotted through the data points. Note that at least for these values of fold amplification, the shape of the fold relative to the initial x-coordinates of nodal points remains perfectly sinusoidal. Plotted relative to current x-coordinates, the shape is no longer sinusoidal.

sinusoidal form, with twice the wavenumber, passing through the origin at the hinge and inflection points. Consequently, these points are displaced as if the deformation was homogeneous (e.g. Casey and Huggenberger, 1985). The lack of hinge or inflection point migration relative to material points justifies the assumption of most previous numerical modellers that analysis of a single half-wavelength segment is sufficient in symmetric pure shear experiments of perfectly periodic forms.

One model was also made with an initial wavelength to thickness ratio for the sinusoidal perturbation of 66:1 (Fig. 2), again with an amplitude of 1/20 of the layer thickness and with material parameters corresponding to the 50:1 viscosity ratio of Table 2. Initial limb dip was very low (~0.3°) and up to ca. 20% shortening, most of the strain was accommodated by layer-parallel shortening. As the bulk shortening increased, however, a fold shape entirely reflecting the introduced perturbation developed and again hinge and inflection points remained fixed to the same material points throughout the experiment. No tendency was observed to develop forms more closely reflecting the dominant wavelength.

The initial amplification rates for the models of Figs. 1(b) and 2, measured as the slope of the near-perfect linear fit between $\ln(A/A_o)$ and logarithmic strain up to strain values of 0.05 are closely predicted by Eq. (29) of Fletcher (1977), derived from an exact first-order analysis of folding for incompressible perfectly viscous materials (Fig. 5b). This demonstrates that, at least for the range of parameters considered in Table 2, the observed behaviour is adequately described by viscous theory and the elastic influence on fold initiation is weak, as already suggested by Biot (1961).

The effects of increasingly elastic behaviour on fold amplification and shape for periodic forms are investigated in Figs. 6 and 7, for parameters as listed in Table 3. Since Deborah numbers are unknown for the earlier study of Zhang et al. (1996), it is possible that the distinctly different results obtained reflected a greater importance of elasticity than for the parameters employed in Fig. 1. However, Fig. 6 demonstrates that even when the elastic strain in the layer is important ($De_l = 0.25$; see first column of Table 3), hinge and inflection points still remain fixed to the same material points. The 33 half wavelengths are preserved throughout the experiments (up to ~50% shortening), similar to Fig. 1. Increasing the elastic component markedly increases the growth rate for the short initial wavelength (six times layer thickness), which consequently leads to different final fold shapes, as seen in Fig. 7. A simple comparison of the first-order, thin-plate approximate solutions of Biot (1961) for an elastic or viscous plate in a viscous matrix can qualitatively explain the observations. Fig. 8 predicts that the elastic effects should first be noticeable for model (c) in Figs. 6 and 7 and that the growth rate for shorter wavelengths around six times layer thickness should increase dramatically as this elastic component becomes more important from models (c) to (b) to (a).

Models starting with an initial bell-shaped perturbation should provide a more sensitive test of elasto-viscous folding behaviour, since the shape at any time reflects the amplification of a wide range of initial wavelengths (Biot et al., 1961; Mancktelow and Abbassi, 1992). The results of Zhang et al. (1996) again show a strong tendency to develop near dominant wavelengths

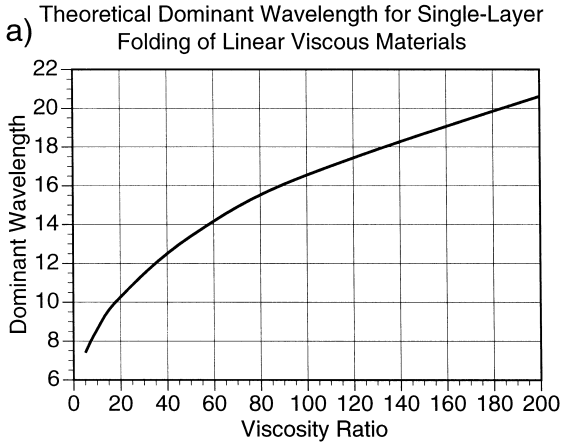

Fig. 5. (a) Dominant wavelength of single-layer folds for incompressible linear viscous materials, from Fletcher (1974, 1977). Note that the initial periodic perturbation in Figs. 1 and 3 (wavelength/layer thickness = 6) is always smaller than the dominant wavelength, and this difference becomes more marked with increasing viscosity contrast. (b) Corresponding initial (infinitesimal amplitude) growth rate for the dominant wavelength, as well as the initial growth rate for a fold with wavelength/layer thickness of 6 and 66. Data values determined from the experiments of Figs. 1(b) and 2 for the growth rate up to $\varepsilon = -0.05$ are also plotted, and agree well with the theoretical curve despite the differences in material properties (compressible elasto-viscous vs incompressible viscous).

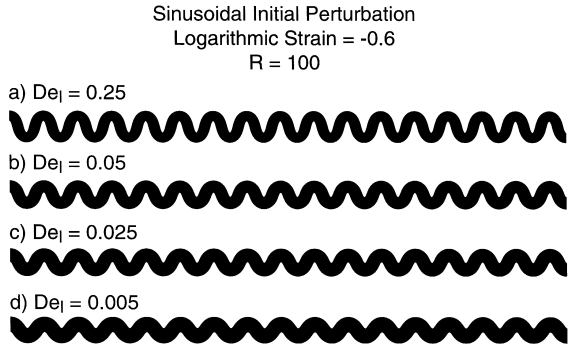

Fig. 6. Amplification of an initial periodic perturbation identical to Fig. 1(b) for $R = 100$ and different Deborah numbers (Table 3). Increasing Deborah numbers correspond to an increasingly important elastic influence on the rheology.

along the length of the layer at shortening values above ~15% (Fig. 9). In contrast, the results from the current FEM modelling (Fig. 10) are very similar in form to those observed in both analogue scale-model experiments (Cobbold, 1975; Abbassi and Mancktelow, 1992) and earlier FEM studies of purely viscous materials (Cobbold, 1977). Propagation along the layer away from the central introduced perturbation is slow and progressive, rather than developing rapidly above some threshold as suggested by Fig. 9. Power-law viscous behaviour (Fig. 11) further accentuates this localization, weakening the tendency to develop adjacent synforms to the initial antiformal perturbation. The gradual serial addition of structures along the layer away from the initial perturbation is well seen in Fig. 12, where shortening has been maintained to values of around −1.3 logarithmic strain (~73% shortening). A striking feature is that although folds are added serially, the final internal shape in the fold packet is nearly perfectly periodic and of constant amplitude. The only indication of progressive development is the change in layer thickness along the folds, particularly marked at lower viscosity contrast.

The influence of increasingly elastic behaviour (i.e. increasing Deborah number) during amplification on an isolated bell-shaped perturbation is demonstrated in Fig. 13. Overall, the effect is to further localize the folding and decrease the amplitude for the more elastic models. Again this can be qualitatively understood by reference to Fig. 8. Since the initial wavelength distribution in a bell-shaped perturbation decreases exponentially from infinite wavelength (e.g. Abbassi and

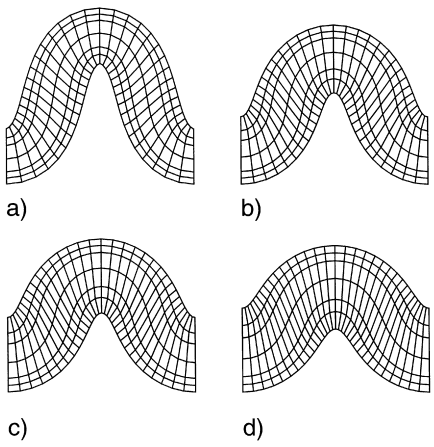

Fig. 7. Enlarged view of the fold shapes developed in Fig. 6 for different Deborah numbers in the layer.

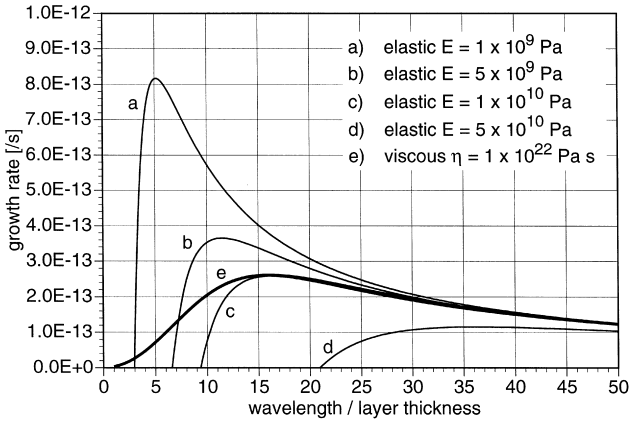

Fig. 8. Comparison of predicted growth rates from infinitesimal-strain thin-plate theory for an elastic or viscous plate in a viscous matrix (e.g. Biot, 1961), for a constant imposed strain rate of 10^{-14} s^{-1} as in the models. Values (a) to (d) correspond to the elastic properties of the corresponding layers in Figs. 6 and 7, while (e) is for a plate with the viscous rheology common to all these models. The side load necessary to calculate curves (a) to (d) is taken as $P = -4\eta\dot{\varepsilon}_{xx}$, following Biot (1961).

Mancktelow, 1992, Fig. 5), promoting growth of these initially lower-amplitude shorter wavelengths by increasing the elastic behaviour will result both in a lower growth of the total isolated form (at least initially) and in a narrower shape, as seen in Fig. 13. In Fig. 14, a comparison is made between shapes developed from the same initial perturbation for a ratio in Young's modulus between layer and matrix of 2:1 (Table 2) and 10:1 (Table 5), for similar Deborah numbers, from which it can be seen that differences in elastic modulus ratio in this range do not affect the overall fold shape.

Single-wavelength periodic and isolated bell-shaped perturbations are useful for assessing the factors controlling fold amplification and for direct comparison with analytical theory, but they are not very realistic. Natural layers have a much more irregular spectrum of irregularities, for which the most extreme example is a completely uncorrelated random distribution. Two such random distributions were computer generated, one offset relative to the other such that there is a section common to both (indicated by the arrows on

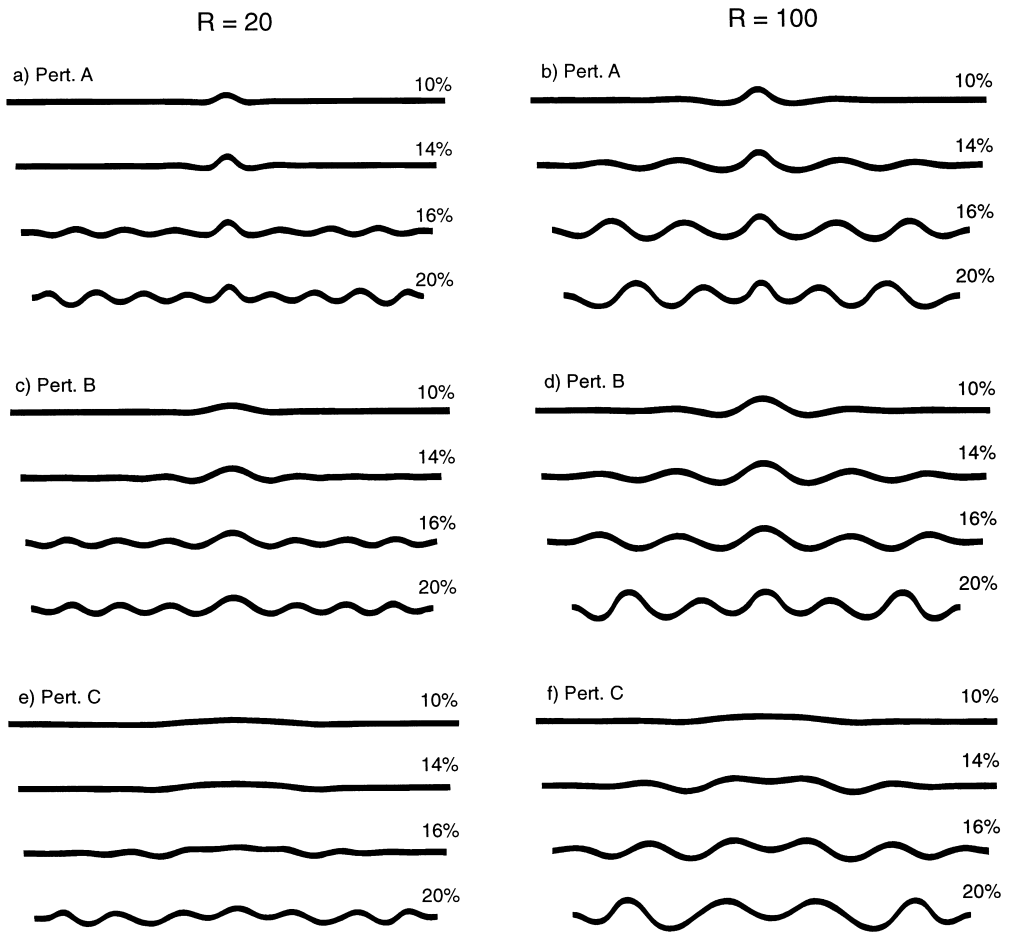

Fig. 9. Reproduction of Fig. 5 from Zhang et al. (1996) showing FLAC models of the development of folding in elasto-viscous materials from an isolated initial perturbation at viscosity contrasts of 20 and 100. Initial amplitude of the central perturbation was 0.7 of layer thickness. Material properties are listed in Table 1.

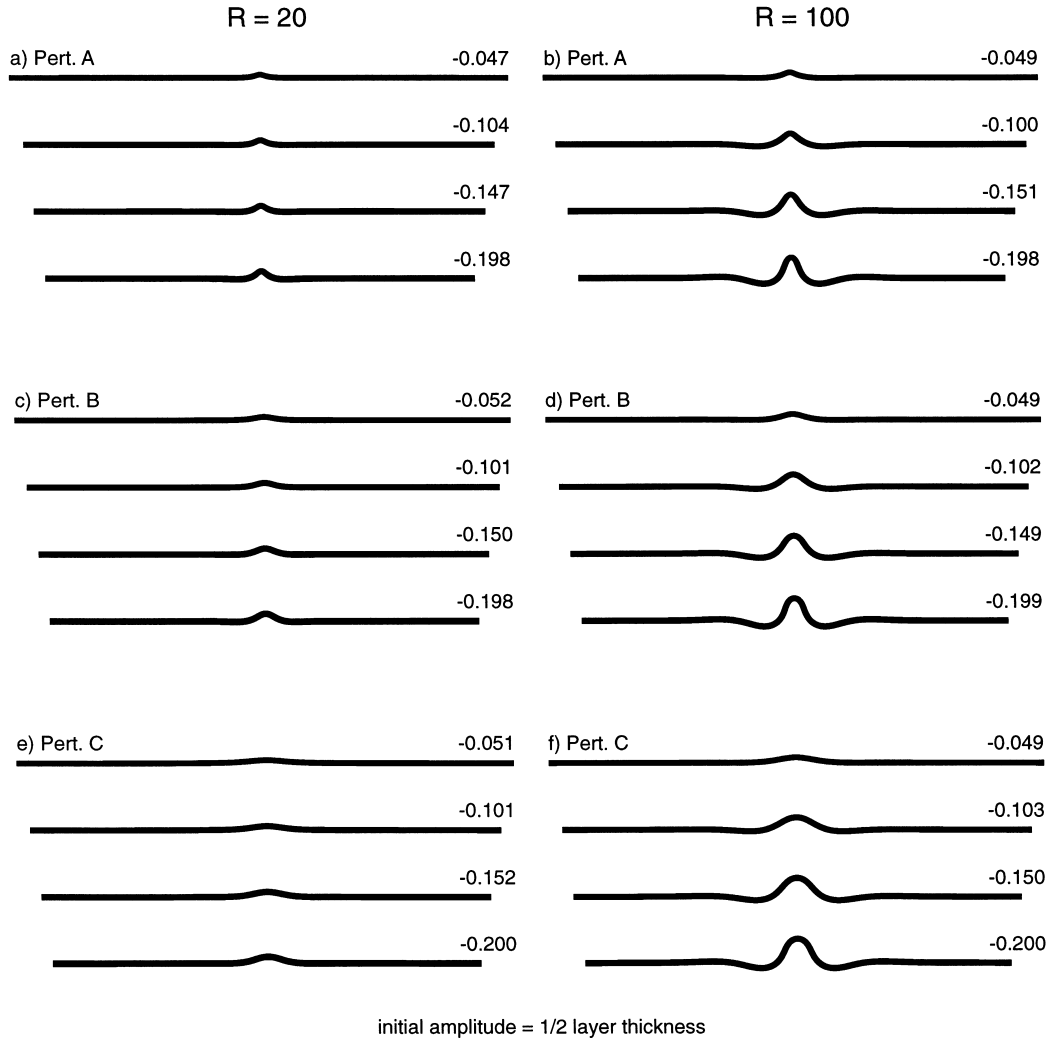

Fig. 10. FEM models directly comparable to the FLAC models of Fig. 9 for different values of bulk shortening (given as logarithmic strain values). Material properties are listed in Table 2. Initial amplitude of the bell-shaped central perturbation was 1/2 of layer thickness. Perturbations. A, B, and C correspond exactly to those employed in Abbassi and Mancktelow (1992). Note the absence of a sudden propagation sideways along the layer at higher values of bulk shortening and thus the tendency to greater localization.

Fig. 15). These were then used as initial perturbations, scaled so that the maximum deviation to either side of the mean surface was either 1/20 or 1/200 of the layer thickness. In Fig. 16, the effects of the different initial distributions, the maximum perturbation amplitude and the viscosity contrast are demonstrated for dominantly viscous materials ($De < 10^{-2}$, see Table 2). Several important observations can be made.

1. An initially random distribution does not immediately lead to a periodic form reflecting the dominant wavelength, although, as might be expected, this tendency does increase with increasing viscosity contrast in conjunction with decreasing initial perturbation amplitude (Biot, 1961).
2. The effect of the common segments in the two different distributions (Fig. 16a and b) can be readily recognized, demonstrating again the local, non-correlated nature of fold initiation and amplification. The segment from Fig. 16(a) could be cut out and overlaid in the corresponding position of Fig. 16(b) and there would be no significant difference.
3. A qualitative comparison with natural single layer folds indicates that the long wavelength forms characteristic of viscosity contrasts greater than 100:1 are uncommon (e.g. Sherwin and Chapple, 1968). Obviously there are cases where such large viscosity contrasts may occur (e.g. calc-silicate layers in marbles), but the contrast in behaviour is then so great that plasticity effects should also be considered (e.g. Biot, 1961; Chapple, 1969). Smith

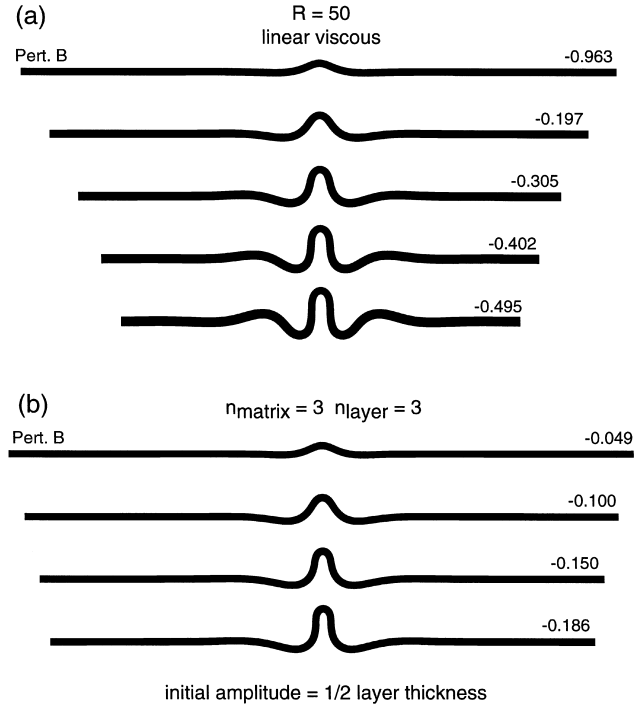

Fig. 11. (a) Amplification of Perturbation B in elasto-linear viscous materials with viscosity ratio of 50:1 (material properties in Table 2). Initial perturbation amplitude is 1/2 of the layer thickness. Note the weak tendency to sideways fold propagation. (b) Amplification of Pert. B in elasto-power law viscous materials with effective viscosity ratio of 50:1 for the basic state of the bulk deformation (material properties in Table 4). Initial perturbation amplitude is 1/2 of the layer thickness. Except for the non-linear viscous property, parameters are the same as Figs. 10 and 11(a). Note the faster growth rate and stronger localization in non-linear viscous materials, with only a weak tendency to develop flanking synforms compared to Figs. 10 and 11(a). The FEM model failed to converge to desired tolerances at higher bulk shortening due to the large distortion of the grid in the inner hinge of the fold.

(1979) has shown that, for very strong power-law behaviour (which approaches plastic behaviour for stress-exponents $n \gg 1$), low wavelength/thickness folds can still develop even when the effective viscosity contrast between layer and matrix is large.

4. Not surprisingly, smaller initial amplitude leads to a smoother overall shape. In the case of high viscosity contrast, the finite fold shape is not greatly altered. However, for lower viscosity contrast (e.g. 50:1), the small initial amplitude leads to much greater layer parallel thickening prior to the 'explosive' phase of fold development (e.g. Biot, 1961; Ramberg, 1964; Hudleston, 1973; Abbassi and Mancktelow, 1992) and thus to quite different final fold shapes at high strain (Fig. 17). In this case, longer wavelength components in the initial distribution dominate the final form and the folds at high bulk shortening show similarities to those developed in higher viscosity contrast experiments with larger initial perturbation amplitudes (e.g. 200:1 in Fig. 16a).

These observations are similar for elasto-power-law viscous rheologies (Fig. 18). The differences that are observed can be directly correlated with the increased growth rate and shorter dominant wavelength developed for folding in non-linear viscous materials (e.g. Fletcher, 1974; Smith, 1977). For the same (effective) viscosity contrast, layer-parallel shortening is therefore less important and the influence of decreasing the initial perturbation amplitude is reduced. However, the general principles are similar to those established for linear viscous behaviour (Fig. 16) and recognition of non-linear behaviour from fold shape alone is difficult (compare Fig. 16a and 18). Lan and Hudleston (1991, 1995, 1996) showed that the shape of high-amplitude folds is sensitive to the degree of non-linear behaviour, becoming sharper-hinged as the power-law exponent increases, but this shape effect is not immediately apparent in the models of Fig. 18.

The influence of increasingly elastic behaviour (i.e. increasing De) on fold development, for the same initial random distribution and linear viscosity contrast, is shown in Fig. 19. As discussed earlier with reference to Fig. 8, increasing the elastic contribution promotes faster growth of shorter wavelengths. It also results in a narrower bandwidth of strongly amplified wavelengths, resulting in greater selectivity during fold growth from the initial random perturbation. A shorter wavelength, more regularly periodic wave train is therefore developed as the Deborah number is increased from Fig. 19 (d) to (a). The faster growth rates also reduce the influence of the initial perturbation amplitude (compare Fig. 20a, b with Fig. 17). However, the influence of the initial distribution is still evident, as is demonstrated by comparing the identical segments forming the right and left halves of Fig. 19a and c, respectively (distributions 1 and 2 in Fig. 15).

There are 20 inflection points defining 19 arcs (or $9\frac{1}{2}$ 'waves') in Fig. 19(a). Relative to the initial layer length (198 units) and thickness (2 units), this corresponds to an average 'initial fold wavelength' of 10.4. However, rapid fold growth in this model only sets in after ca. -0.2 logarithmic strain, preceded by a period of dominantly layer-parallel shortening. The average fold wavelength is then around 7 times the layer thickness at the time of transition between dominantly layer-parallel shortening and buckling modes of deformation. This value is larger than the value of around 5 that can be read from Fig. 8 for the appropriate curve (a) for elastic buckling of a single layer in a viscous matrix. However, these curves were calculated assuming that the load in the layer attains a value appropriate for steady viscous flow ($\sigma_{xx} = 4\eta_l\dot{\varepsilon}_{xx} = 400$ MPa). In practice, buckling occurs in the elasto-viscous layer

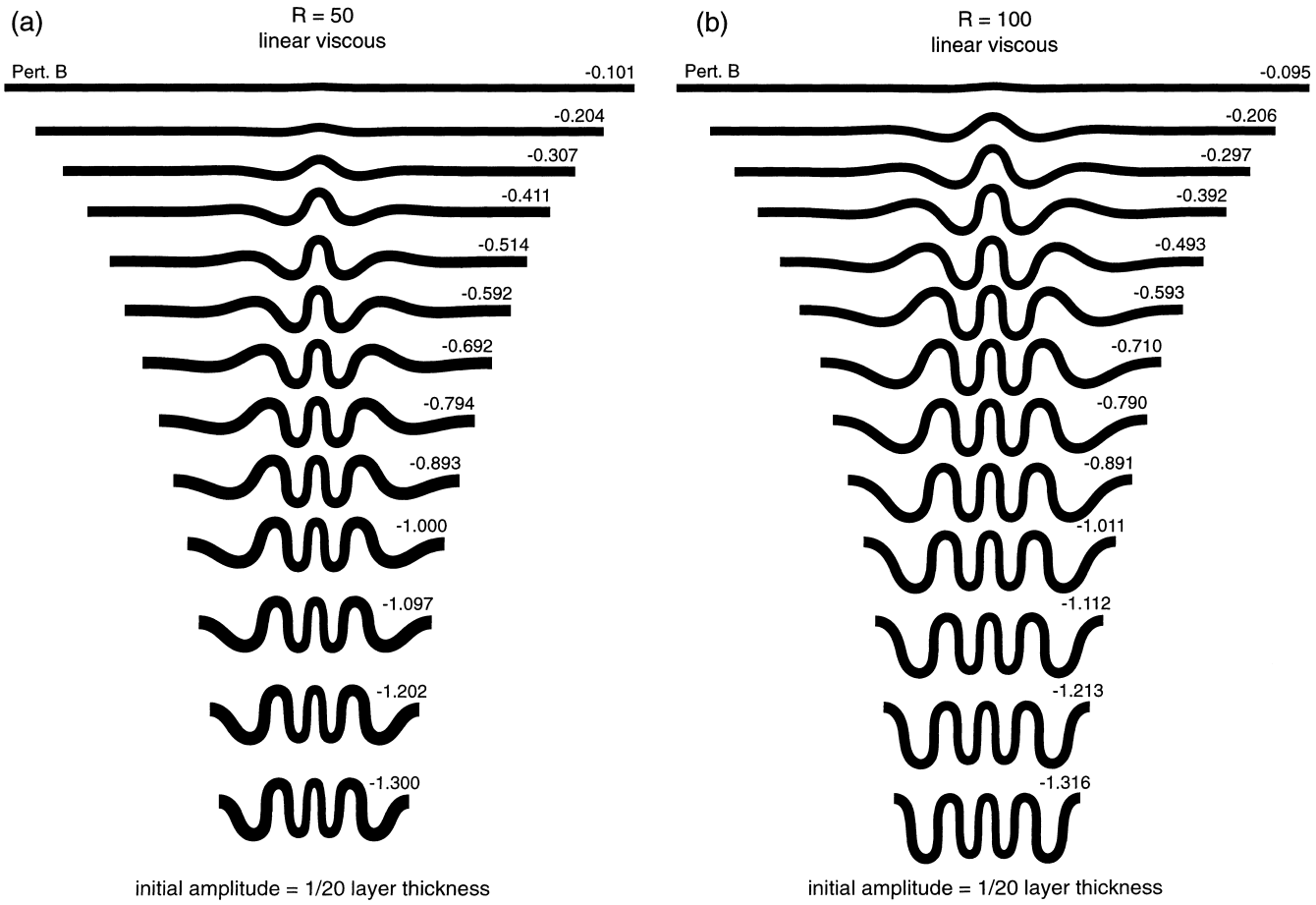

Fig. 12. Amplification and lateral propagation of initial bell-shaped Pert. B for elasto-(linear)viscous materials with viscosity ratios $R = 50$ and 100, to a maximum shortening of $\varepsilon = -1.3$ (~73% shortening). Note the eventual development of a perfectly periodic fold packet of constant amplitude, although the folds themselves are serially developed. Initial perturbation amplitude was only 1/20 of the layer thickness. Material properties listed in Table 5.

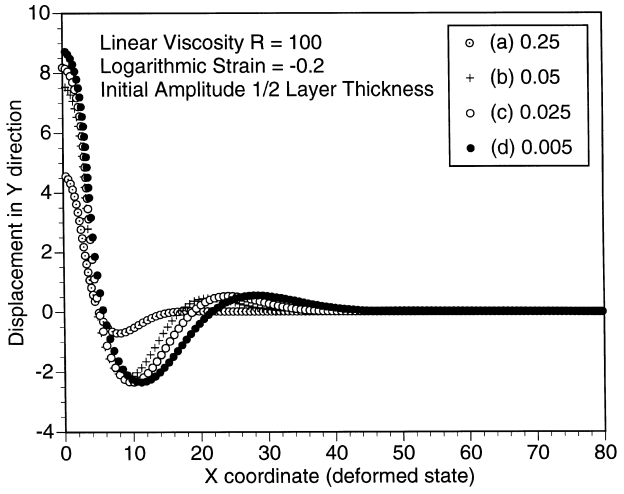

Fig. 13. Influence of increasing elasticity on folding developed from an initial isolated perturbation. (a)–(d) refer to Deborah numbers (Table 3) and correspond to the identical values in Fig. 6.

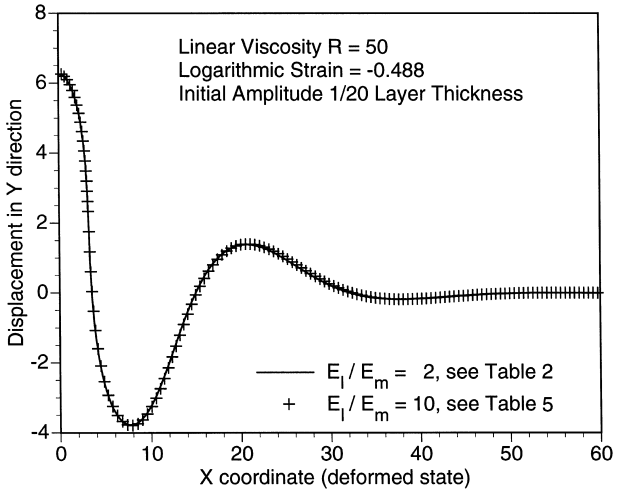

Fig. 14. Models demonstrating the lack of influence of an increased contrast in Young's modulus between layer and matrix.

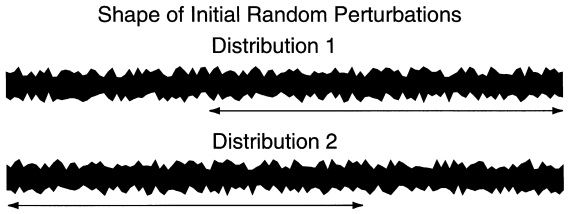

Fig. 15. Random initial distributions 1 and 2 with exaggerated amplitudes for clarity. In practice, maximum amplitudes are either 1/20 or 1/200 of the layer thickness. The section of the sequence that is common to both distributions is indicated by the arrow.

of Fig. 19(a) well before this value is reached, peaking at an average value of ~180 MPa along the mid-line of the layer at logarithmic strain ~−0.2. With this value, curve (a) in Fig. 8 would peak at a wavelength/thickness ratio of ~7.6, close to the observed value. This suggests, perhaps not surprisingly, that it is the elastic component of the rheology that determines the

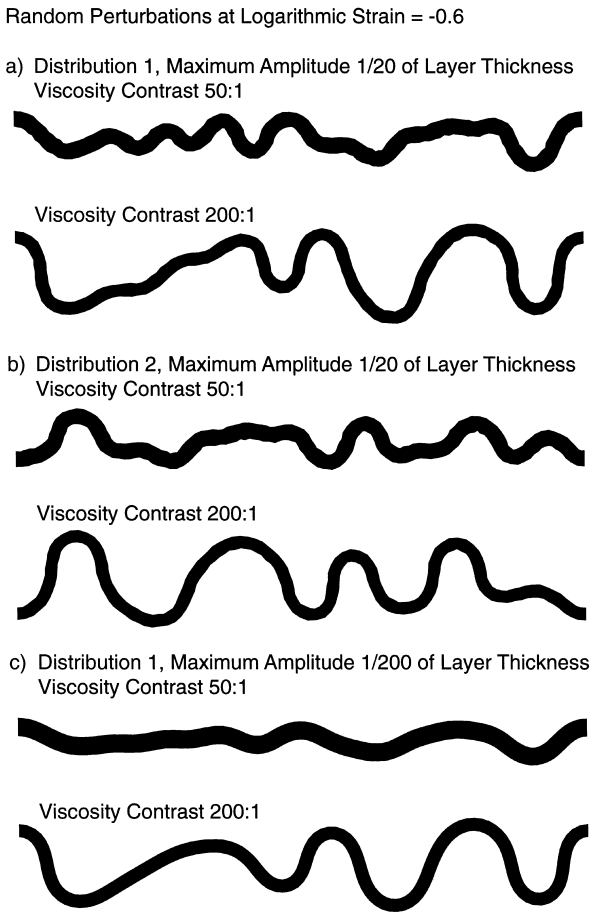

Fig. 16. Single-layer folds developed in elasto-(linear)viscous materials with initial random perturbation distributions 1 and 2 at $\varepsilon = -0.6$ (~45% shortening). Viscosity ratio is either 50:1 or 200:1 and other parameters as in Table 2.

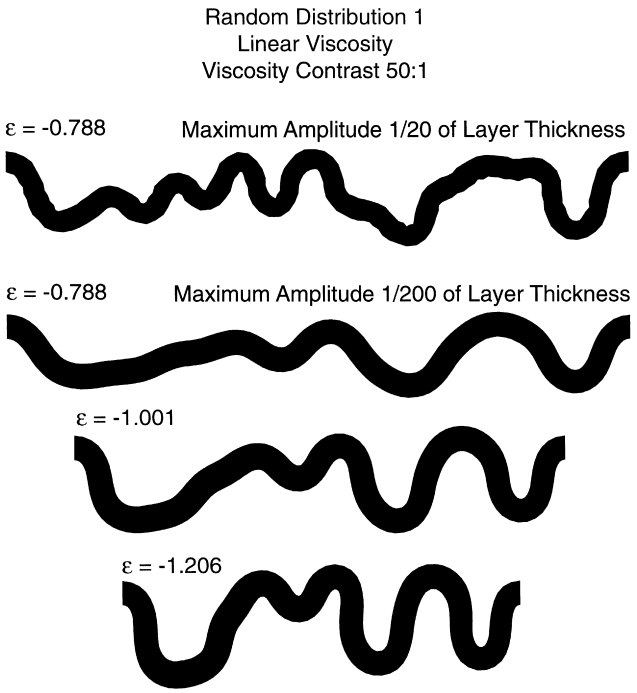

Fig. 17. Models demonstrating the influence of initial perturbation amplitude on the final geometry of single-layer folds. All parameters are the same except for initial maximum amplitude (distribution 1, viscosity ratio 50:1, other values see Table 2.

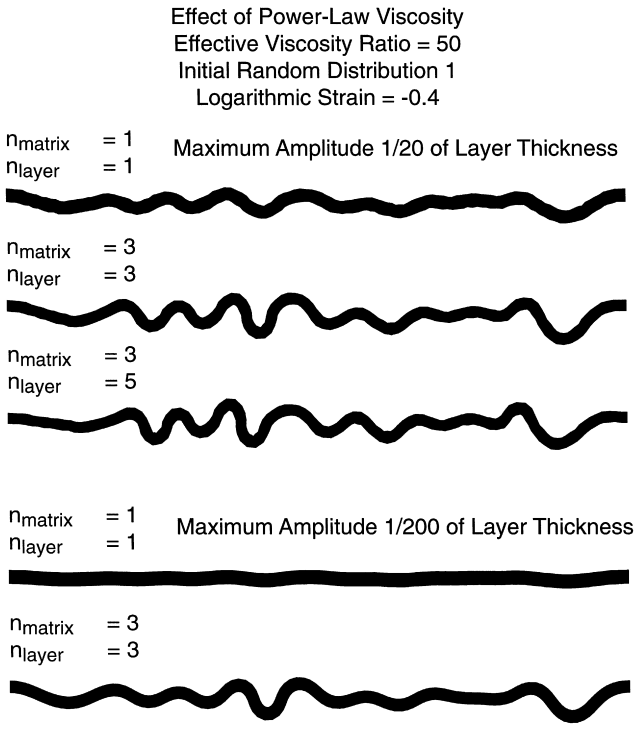

Fig. 18. Single-layer folds developed in elasto-(power-law)viscous materials with initial random perturbation distribution 1 at $\varepsilon = -0.4$ (~33% shortening). Viscosity ratio is 50:1, other parameters as in Table 4.

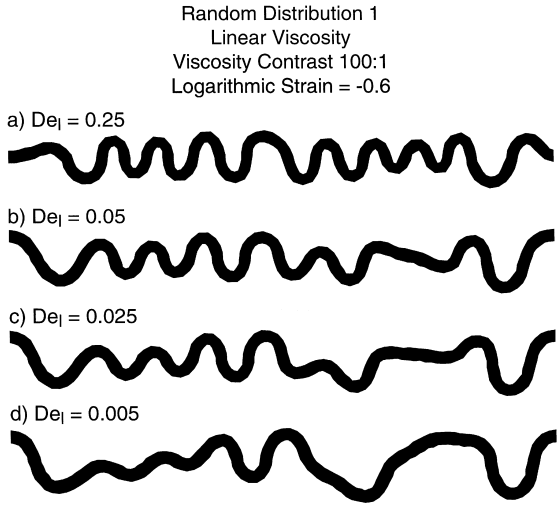

Fig. 19. Effect of increasing Deborah numbers (i.e. increasing elastic influence) on the fold geometry developed from initial random distribution 1 (see Fig. 15), with maximum initial amplitude 1/20 of the layer thickness. Material parameters are the same as for Figs. 6 and 13, and are listed in Table 3.

wavelength in the elasto-viscous layer for such high Deborah numbers.

8. Discussion

Overall, the results for folds developed from periodic and isolated initial perturbations in elasto-viscous materials are similar to earlier analytical and numerical modelling results for purely viscous behaviour and the influence of increasingly elastic behaviour can be qualitatively predicted from approximate theories for elastic and viscous plates in a viscous matrix (e.g. Fig. 8). The reason for the marked differences from the only earlier directly comparable study of Zhang et al. (1996) is not readily apparent. Since their results could not be reproduced in this study, even for a very wide range of elasto-viscous material parameters, the difference must lie in the different numerical modelling techniques employed. The similarity of the current results to analogue scale-model experiments using elasto-viscous materials (e.g. Cobbold, 1975; Abbassi and Mancktelow, 1992) provides independent support for the finite-element models presented here.

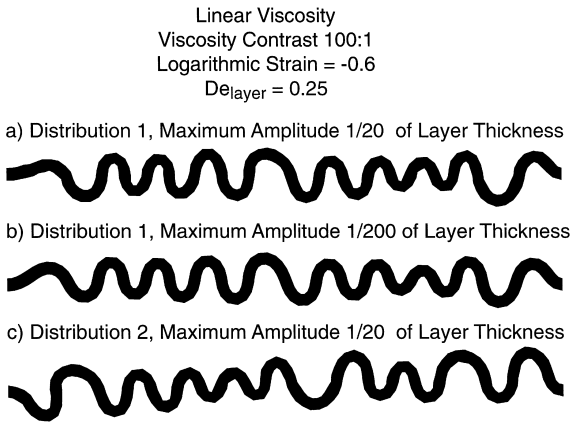

Fig. 20. Influence of initial random perturbation geometry on folding at high Deborah number (De = 0.25). Material properties are the same as Fig. 19(a).

As discussed by Biot (1961) in his consideration of the bandwidth of fold amplification and associated wavelength selectivity, total amplification needs to be on the order of 1000 for a single dominant wavelength to become well-established from an initial random distribution. This will never be achieved in natural examples. As again confirmed in Figs. 16 to 18, wavelength selectivity from the initial broad band available in the random perturbation only occurs at low limb dip and is rapidly 'frozen in'. A simple calculation establishes that the required maximum amplitude of initial irregularities is unrealistically small for amplification on the order of 1000 to be achieved before such low limb dips are exceeded (see appendix of Mancktelow and Abbassi, 1992). Natural single-layer folds have wavelengths suggesting moderate viscosity contrasts (e.g. Sherwin and Chapple, 1968) and the ratio of layer-parallel shortening to fold amplification scales as the square of the limb dip (Ramberg, 1964). Taken together this implies predominance of layer-parallel shortening over fold amplification in natural situations where the initial perturbations could be of the order necessary for establishing a clear periodic form of narrow bandwidth. Strongly elastic behaviour does promote a more periodic form, but the effect only becomes marked for high Deborah numbers requiring either a low elastic shear modulus (e.g. 10^9 Pa for the examples considered here), high effective viscosities or fast strain rates. Even then, the initial random distribution can still be recognized in the final fold form. For most natural single-layer folding, the effects of initial irregularities will never be overcome, as reflected in the only quasi-periodic forms observed, which are similar to those produced in this study from random initial perturbations of small but finite amplitude.

9. Conclusions

The FEM results reaffirm the earlier observations of Cobbold (1975, 1977), Williams et al. (1978) and Abbassi and Mancktelow (1992) that the initial perturbation geometry exerts a strong influence on the geometry of finite-amplitude folds. At low strain rates and stresses, considering a more realistic compressible elasto-viscous rheology as appropriate to natural rocks does not significantly change the observations when compared to earlier studies for purely viscous behaviour

(Biot, 1961). An initial perfectly periodic perturbation amplifies and modifies its shape during amplification, but hinge and inflection points remain fixed to material points, which deform as if they were passive markers in a homogeneous deformation (Casey and Huggenberger, 1985). Folds develop serially away from an isolated initial perturbation to eventually develop a periodic form of nearly constant amplitude, despite the sequential development. Increasing the elastic influence on the rheology changes the amplification rate and fold shape, but does not modify these fundamental observations.

The geometry of initial irregularities is still discernible in the finite amplitude folds even when the distribution is random. The effect of initial perturbation shape has only a quite local range, so that the same random sequence produces the same finite fold shape even when adjacent sequences are different. The quasi-periodic form of most natural fold trains is very similar to those produced in the numerical models with random initial perturbations, suggesting that in nature it is also the initial perturbation shape that determines the irregularity observed in the final fold geometry.

Acknowledgements

Discussions with Yuri Podladchikov, Stefan Schmalholz, Markus Härri, and Martin Casey helped both the formulation and interpretation of the numerical models. Thomas Kenkmann provided a first template input file from his work with MARC, that provided the starting point for this study. Thorough reviews by Peter Cobbold and Peter Hudleston are gratefully acknowledged.

Appendix A

A.1. Material properties

R is the (effective) viscosity ratio, E_l and E_m the Young's elastic moduli, η_l and η_m the viscosities for linear viscous materials, De_l and De_m the Deborah numbers ($De = \eta\dot{\varepsilon}/G$, where G is the elastic shear modulus), A_l and A_m the pre-exponential factor in the power-law relationship $d\varepsilon/dt = A\sigma^n$, with n_l and n_m the stress exponents in this same relationship ($=1$ for linear viscous). In all cases, the subscripts l and m refer to the layer and matrix, respectively. The Poisson's ratio is always 0.25, a Maxwell elasto-viscous model is employed and the compressibility is assumed to be only elastic. Although constants are given in standard SI units (i.e. Pa), in practice they are entered into the FEM program in stress units of MPa. For power-law rheologies with higher stress exponents, time is also considered in units of 10^{10} s. These measures are necessary to avoid numerical under- and overflow and as general good numerical programming practice, avoiding operations involving (unnecessarily) large and small numbers.

A.2. Solution procedures, element geometry and program parameters

MARC is marketed by MARC Analysis Research Corporation, 260 Sheridan Avenue, Suite 309 Palo Alto, CA 94306 USA (see Internet web pages www.marc.com or www.marc.de). It is one of several commercial non-linear finite element packages that have been well-tested both against each other and against experimental results (e.g. Fanous et al., 1990). These programs have a wide application in general engineering, in the nuclear industry, and in materials processing (e.g. in modelling high-strain superplastic forming of components). Links to many published articles are provided by the web pages listed above. The MARC program was developed on the basis of the displacement method, with force–displacement relations addressed through the stiffness of the system. The program copes with non-linearities due to material rheology (e.g. elasto-viscous and/or power-law creep rheology), geometry (large displacements, strains and rotations, e.g. Hibbitt et al., 1970), and boundary conditions. In a non-linear problem, the system equations must be solved incrementally. There are several solution procedures available in MARC for the solution of non-linear equations, but all models presented here use the full Newton–Raphson method (e.g. Press et al., 1986, p.254). The convergence criterion is based on the magnitude of the maximum residual load compared to the maximum reaction force. This is appropriate since the residuals measure the out-of-equilibrium force, which should be minimized. In MARC, creep is represented by a Maxwell model. To allow direct input of typical experimental data, the parameters input for isotropic materials are those appropriate to a uniaxial test, namely the Young's modulus, the Poisson's ratio and the pre-exponential constant and stress exponent for power-law creep of the form $\dot{\varepsilon} = A\sigma^n$. Internally, these values are then converted to those appropriate to an effective stress vs effective strain rate formulation based on the second invariants of the tensors (e.g. Ranalli, 1995, p.76).

All experiments were for plane strain, with a default element thickness of 1 unit. Element type 11 of

MARC was utilized, which is a four-node, isoparametric, arbitrary quadrilateral written for plane strain applications. The stiffness of this element is formed using four-point Gaussian integration. An assumed strain interpolation formulation is used that significantly improves the behaviour of this element during bending and an optional integration scheme is also used, which imposes a constant dilatational strain on the element. This is equivalent to a selective integration where the four internal Gaussian points are used for the deviatoric contribution of strain and the centroid for the dilatational contribution. Constant dilatational elements are recommended for large strain creep analysis because near incompressibility can produce overly stiff behaviour and volumetric locking in conventional elements due to overconstraints, with consequent degradation of accuracy. The large displacement option was invoked to signal the program to calculate the geometric stiffness matrix and the initial stress stiffness matrix. This parameter automatically switches on the residual load correction option. The large strain plasticity option is also invoked, so that effects of the change in the metric tensor (e.g. Mase, 1970, p. 13) resulting from large inelastic deformations are included. This results in a different stiffness of the structure as well as in a modified calculation of stresses and inelastic strains. This option is used in conjunction with the updated Lagrange procedure, the use of which has two consequences. First, the element stiffnesses are assembled in the current configuration of the element. Second, the stress and strain output is given in the coordinate system which is applicable in the updated configuration of the element. After some experimentation, it was found that the sparse direct solver using the minimum degree algorithm for bandwidth optimization provided the fastest calculation times. Results obtained were indistinguishable from the default profile direct solver using the Sloan algorithm for optimization, but calculation times were improved by around 30%.

References

Abbassi, M.R., Mancktelow, N.S., 1992. Single layer folding in non-linear materials—I. Experimental study of fold development from an isolated initial perturbation. Journal of Structural Geology 14, 85–104.

Bhalerao, M.S., Moon, T.J., 1996a. Micromechanics of local viscoelastic buckling in thick composites. Composites Part B 27B, 561–568.

Bhalerao, M.S., Moon, T.J., 1996b. On the growth-of-waviness in fiber-reinforced polymer composites: viscoelastic bifurcation and imperfection sensitivity. Transactions of the American Society of Mechanical Engineers 63, 460–466.

Biot, M.A., 1959. Folding of a layered viscoelastic medium derived from an exact stability theory of a continuum under initial stress. Quarterly of Applied Mathematics 17, 185–204.

Biot, M.A., 1961. Theory of folding of stratified viscoelastic media and its implication in tectonics and orogenesis. Geological Society of America Bulletin 72, 1595–1620.

Biot, M.A., 1965. Mechanics of Incremental Deformations. John Wiley and Sons, New York.

Biot, M.A., Odé, H., Roever, W.L., 1961. Experimental verification of the theory of folding of stratified viscoelastic media. Geological Society of America Bulletin 72, 1621–1632.

Biot, M.A., Odé, H., 1962. On the folding of a viscoelastic medium with adhering layer under compressive initial stress. Quarterly Journal of Applied Mathematics 19, 351–355.

Casey, M., Huggenberger, P., 1985. Numerical modelling of finite-amplitude similar folds developing under general deformation histories. Journal of Structural Geology 7, 103–114.

Chapple, W.M., 1969. Fold shape and rheology: the folding of an isolated viscous-plastic layer. Tectonophysics 7, 97–116.

Cobbold, P.R., 1975. Fold propagation in single embedded layers. Tectonophysics 27, 333–351.

Cobbold, P.R., 1976. Fold shapes as functions of progressive strain. Philosophical Transactions of the Royal Society of London A283, 129–138.

Cobbold, P.R., 1977. Finite element analysis of fold propagation—a problematic application? Tectonophysics 38, 339–353.

Cundall, P.A., Board, M., 1988. A microcomputer program for modelling large-strain plasticity problems. In: G. Swoboda (Ed.), Numerical Methods in Geomechanics. Balkema, Rotterdam, pp. 2102–2108.

Dieterich, J.H., Carter, N.L., 1969. Stress history of folding. American Journal of Science 267, 129–154.

Fanous, F., Greimann, L., Rogers, J., 1990. ANSYS 3-D analysis of nuclear steel containment. FEN—Finite-Element-News 5, 28–34.

Fletcher, R.C., 1974. Wavelength selection in the folding of a single layer with power-law rheology. American Journal of Science 274, 1029–1043.

Fletcher, R.C., 1977. Folding of a single viscous layer: exact infinitesimal-amplitude solution. Tectonophysics 39, 593–606.

Fletcher, R.C., 1979. The shape of single-layer folds at small but finite amplitude. Tectonophysics 60, 77–87.

Fletcher, R.C., Sherwin, J.-A., 1978. Arc lengths of single layer folds: a discussion of the comparison between theory and observation. American Journal of Science 278, 1085–1098.

Goodier, J.N., 1946. Cylindrical buckling of sandwich plates. Journal of Applied Mechanics 68, 253–260.

Gough, G.S., Elam, C.F., DeBruyne, N.A., 1940. The stabilization of a thin sheet by a continuous supporting medium. Journal of the Royal Aeronautical Society 44, 12–43.

Hanks, T.C., Raleigh, C.B., 1980. The conference on magnitude of deviatoric stresses in the Earth's crust and upper mantle. Journal of Geophysical Research 85, 6083–6085.

Hibbitt, H.D., Marcal, P.V., Rice, J.R., 1970. A finite element formulation for problems of large strain and large displacement. International Journal of Solids and Structures 6, 1069–1086.

Hudleston, P.J., 1973. An analysis of 'single-layer' folds developed experimentally in viscous media. Tectonophysics 16, 189–214.

Hudleston, P.J., Lan, L., 1993. Information from fold shapes. Journal of Structural Geology 15, 253–264.

Hudleston, P.J., Stephansson, O., 1973. Layer shortening and fold-shape development in the buckling of single layers. Tectonophysics 17, 299–321.

Hunt, G., Mühlhaus, H., Hobbs, B., Ord, A., 1996a. Localized folding of viscoelastic layers. Geologische Rundschau 85, 58–64.

Hunt, G.W., Mühlhaus, H.-B., Whiting, A.I.M., 1996b. Evolution of localized folding for a thin elastic layer in a softening visco-elastic medium. Pure and Applied Geophysics 146, 229–252.

Johnson, A.M., Fletcher, R.C., 1994. Folding of Viscous Layers. Columbia University Press, New York.

Lan, L., Hudleston, P.J., 1991. Finite element models of buckle folds in non-linear materials. Tectonophysics 199, 1–12.

Lan, L., Hudleston, P.J., 1995. A method of estimating the stress exponent in the flow law in rocks using fold shape. Pure and Applied Geophysics 145, 620–633.

Lan, L., Hudleston, P.J., 1996. Rock rheology and sharpness of folds in single layers. Journal of Structural Geology 18, 925–931.

Mancktelow, N.S., Abbassi, M.R., 1992. Single layer buckle folding in non-linear materials—II. Comparison between theory and experiment. Journal of Structural Geology 14, 105–120.

Mase, G.E., 1970. Theory and Problems of Continuum Mechanics. Schaum's Outline Series in Engineering. McGraw-Hill, New York.

Parrish, D.K., 1973. A nonlinear finite element fold model. American Journal of Science 273, 318–334.

Parrish, D.K., Krivz, A.L., Carter, N.L., 1976. Finite-element folds of similar geometry. Tectonophysics 32, 183–207.

Poliakov, A.N.B., Cundall, P.A., Podladchikov, Y.Y., Lyakhovsky, V.A., 1993. An explicit inertial method for the simulation of viscoelastic flow: an evaluation of elastic effects on diapiric flow in two- and three-layers models. In: Stone, D.B., Runcorn, S.K. (Ed.). Flow and Creep in the Solar System: Observations, Modeling and Theory. Kluwer Academic Publishers, Dordrecht, Holland,
pp. 175–195.

Press, W.H., Flannery, B.P., Teukolsky, S.A., Vetterling, W.T., 1986. Numerical Recipes. The Art of Scientific Computing. Cambridge University Press, Cambridge.

Price, N.J., Cosgrove, J.W. 1990. Analysis of Geological Structures. Cambridge University Press, Cambridge.

Ramberg, H., 1963. Fluid dynamics of viscous buckling applicable to folding of layered rocks. American Association of Petroleum Geologists Bulletin 47, 484–515.

Ramberg, H., 1964. Selective buckling of composite layers with contrasting rheological properties, a theory for simultaneous formation of several orders of folds. Tectonophysics 1, 307–341.

Ranalli, G., 1995. Rheology of the Earth (2nd Ed.). Chapman and Hall, London.

Sherwin, J.-A., Chapple, W.M., 1968. Wavelengths of single layer folds: a comparison between theory and observation. American Journal of Science 266, 167–179.

Smith, R.B., 1975. Unified theory of the onset of folding, boudinage and mullion structure. Geological Society of America Bulletin 86, 1601–1609.

Smith, R.B., 1977. Formation of folds, boudinage, and mullions in non-Newtonian materials. Geological Society of America Bulletin 88, 312–320.

Smith, R.B., 1979. The folding of a strongly non-Newtonian layer. American Journal of Science 279, 272–287.

Stephansson, O., 1974. Stress-induced diffusion during folding. Tectonophysics 22, 233–251.

Stephansson, O., Berner, H., 1971. The finite-element method in tectonic processes. Physics of the Earth and Planetary Interiors 4, 301–321.

Turcotte, D.L., Schubert, G., 1982. Geodynamics—Applications of Continuum Physics to Geological Problems. John Wiley & Sons, New York.

Wilson, D.W., Vinson, J.R., 1983. Viscoelastic analysis of laminated plate buckling. American Institute of Aeronautics and Astronautics Journal 22, 982–988.

Whiting, A.I.M., Hunt, G.W., 1997. Evolution of nonperiodic forms in geological folds. Mathematical Geology 29, 705–723.

Williams, J.R., Lewis, R.W., Zienkiewicz, O.C., 1978. A finite-element analysis of the role of initial perturbations in the folding of a single viscous layer. Tectonophysics 45, 187–200.

Zhang, Y., Hobbs, B.E., Ord, A., Mühlhaus, H.B., 1996. Computer simulation of single-layer buckling. Journal of Structural Geology 18, 643–655.